First half-life measurement of a low-lying isomer in ^{37}Si

T. H. Ogunbeku [1,2,*] B. P. Crider,[1] S. N. Liddick,[2,3] B. A. Brown,[2,4] A. Chester [2] K. L. Childers,[2,3,†] P. Chowdhury,[5] E. Lamere,[5,‡] R. Lewis,[2,3] B. Longfellow,[2,4,§] R. S. Lubna,[6] S. Lyons [2,‖] S. K. Neupane,[7] D. Perez-Loureiro,[7] C. J. Prokop,[8] A. L. Richard,[2,§] U. Silwal [1] D. P. Siwakoti,[1] D. C. Smith,[1] M. K. Smith,[2] and Y. Xiao[1,¶]

[1]*Department of Physics and Astronomy, Mississippi State University, Mississippi State, Mississippi 39762, USA*
[2]*National Superconducting Cyclotron Laboratory, Michigan State University, East Lansing, Michigan 48824, USA*
[3]*Department of Chemistry, Michigan State University, East Lansing, Michigan 48824, USA*
[4]*Department of Physics and Astronomy, Michigan State University, East Lansing, Michigan 48824, USA*
[5]*Department of Physics and Applied Physics, University of Massachusetts Lowell, Lowell, Massachusetts 01854, USA*
[6]*Facility for Rare Isotope Beams, Michigan State University, East Lansing, Michigan 48824, USA*
[7]*Department of Physics and Astronomy, University of Tennessee, Knoxville, Tennessee 37996, USA*
[8]*Los Alamos National Laboratory, Los Alamos, New Mexico 87545, USA*

Background: The appearance of isomeric states in neutron-rich nuclei can provide a wealth of information on the underlying nuclear configurations as a progression is made from stable to exotic nuclei. These states can be characterized by measuring the half-lives and transition probabilities associated with their deexcitations. Recent studies on neutron-rich Si isotopes near $N = 20$ and approaching $N = 28$ have revealed states with intruder configurations resulting from multiple-particle, multiple-hole excitations across the closed shell gaps. These intruder states appear at low excitation energies along the Si isotopic chain, pointing to a diminished shell gap at $N = 28$.

Purpose: The experiment was set up to directly measure the half-lives of isomeric states in neutron-rich nuclei populated via β decay.

Methods: ^{37}Al and ^{38}Al isotopes were produced in the projectile fragmentation reaction of a ^{48}Ca primary beam at NSCL. The isotopes were implanted into a CeBr$_3$ detector, populating excited states of interest in ^{37}Si following their β^- and β^-n decay, respectively. Ancillary arrays of HPGe and LaBr$_3$(Ce) detectors were used to detect β-delayed γ rays. The half-lives of populated isomeric states were measured using the $\beta - \gamma$ timing method.

Results: The half-life of the 68-keV $(7/2_1^-)$ state in ^{37}Si was measured for the first time as 9.1(7) ns, while that of the 156-keV $(3/2_1^-)$ state was 3.20(4) ns, consistent with a previously reported value. The reduced transition probabilities and transition matrix elements associated with the γ-ray decay from these excited states to the $(5/2_1^-)$ ground state were extracted and agree with results from shell model calculations.

Conclusions: The characterization of the $(7/2_1^-)$ and $(3/2_1^-)$ states in ^{37}Si validates shell model predictions of low-lying nanosecond isomers in neutron-rich odd-A Si isotopes approaching the $N = 28$ shell gap.

I. INTRODUCTION

Shell evolution in exotic nuclei is a consequence of the monopole interaction of nuclear forces—predominantly the

---

*Corresponding author: hezekiahogunbeku@gmail.com

†Present address: Remote Sensing Laboratory - Nellis, Las Vegas, Nevada 89191 USA.

‡Present address: Environment, Health and Safety, Massachusetts Institute of Technology, Cambridge Massachusetts, 02139, USA.

§Present address: Lawrence Livermore National Laboratory, Livermore, California 94550, USA.

‖Present address: Pacific Northwest National Laboratory, Richland, Washington 99352, USA.

¶Present address: Department of Chemistry, University of Kentucky, Lexington, Kentucky 40506, USA.

tensor force—which drives the collapse and subsequent disappearance of the magic nature of classical shell gaps and the appearance of new ones [1,2]. This is particularly evident in the reordering of shell model configurations of neutron-rich nuclei including those located near the $N = 28$ shell gap, which is a closed shell. Shell gaps in these nuclei are diminished due to the spin-orbit interaction leading to the enhancement of cross-shell excitations across the gaps, accompanied by the appearance of intruder states that lie at low excitation energies or even become the ground states. The observation and characterization of low-lying isomeric states provide information on the microscopic structure of the nuclei in which they appear and can provide insight into shell evolution along isotopic chains as nuclei become more exotic.

The first indication of the disappearance of the $N = 28$ shell gap was observed in ^{44}S, with a low 2_1^+ excitation

energy of 1297(18) keV, characterized by a large quadrupole transition probability of $B(E2 : 0^+_{g.s.} \rightarrow 2^+_1)$ of 314(88) e^2fm^2 [3]. Similar evidence in the downward trend of 2^+_1 excitation energies has been established along the $N = 20$ up to $N = 28$ chains of even-even isotones below ^{48}Ca, including Si [4]. Specifically, the 2^+_1 state in ^{34}Si ($N = 20$) has an excitation energy of 3326 keV [5], compared to the 2^+_1 state in ^{42}Si ($N = 28$), which has an excitation energy of 742(8) keV [6]. The observation of 2^+_1 states with low excitation energies and large quadrupole transition probabilities indicate enhanced quadrupole collectivity, and in some cases, coexisting spherical and deformed 0^+ states [7–10].

Low-lying excited states are also observed in odd-A Si isotopes approaching $N = 28$. The $(3/2^+_1)$ isomer [$T_{1/2} = 5.9(6)$ ns] at 973.8(30) keV in ^{35}Si, which decays to its $(7/2)^-$ ground state [11] differs from the $(3/2^+_1)$ states in ^{37,39}Si, which progressively become lower in energy, and decay by a fast $E1$ to the $(5/2^-)$ ground states and lower-lying excited $(3/2^-_1)$ states. These $(3/2^-_1)$ states are predicted to be nanosecond isomers along with the $(7/2^-_1)$ states in ^{37}Si and ^{39}Si [12,13].

The $(3/2^-_1)$ and $(7/2^-_1)$ states were first established in the level scheme of ^{37}Si following the β^- [14,15] and β^-n [14] decay of ^{37}Al and ^{38}Al, respectively. Further investigation of the structure of ^{37}Si in a ^{9}Be(^{38}Si, ^{37}Si γ) reaction led to the identification of the 156-keV $(3/2^-_1)$ state as a nanosecond isomer with a reported half-life of 3.0(7) ns [12]. Although the $(7/2^-_1)$ state was unplaced in Ref. [12], shell model calculations were reported predicting two low-lying isomeric states in ^{37}Si, including the $(3/2^-_1)$ state.

In this paper, we confirm the observation of the $(7/2^-_1)$ isomeric state and a corresponding γ-ray transition to the ground state of ^{37}Si following the β^-n decay of ^{38}Al. We also measure its half-life for the first time, confirm the half-life of the 156-keV state, and extract reduced transition probabilities for both aforementioned isomeric transitions to the ground state. We then compare the measurements with theoretical results from shell model calculations using the SDPF-MU [16] and SDPF-U-SI [17] interactions, and provide inferences on the shell structure implications of our findings in Sec. IV.

II. EXPERIMENTAL DETAILS

The experiment was carried out at the National Superconducting Cyclotron Laboratory (NSCL) at Michigan State University to study the properties of neutron-rich nuclei located near $N = 28$. Isomeric states in these nuclei were populated following the β decay of radioactive ions produced in the fragmentation of a 140 MeV/u ^{48}Ca primary beam on a 642 mg/cm^2-thick ^{9}Be target at the Coupled Cyclotron Facility (CCF) of the NSCL.

Radioactive ions of interest were selected from the fragmentation reaction products using the A1900 fragment separator [18]. The selected ions of interest were then delivered to the experimental end station as a secondary cocktail beam centered around ^{33}Na, which accounted for $\approx5\%$ of the total transmitted ions, as shown in the particle identification map in Fig. 1.
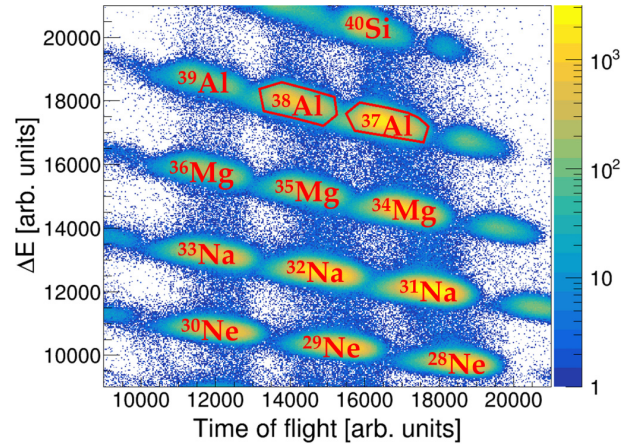

FIG. 1. Particle identification (PID) map for ions delivered to the experimental end station. The plot consists of the energy loss (ΔE) in the first PIN detector and the time-of-flight (TOF) between a scintillator in the A1900 fragment separator and the first PIN detector. ^{37,38}Al ions of interest are highlighted with red graphical cuts.

The secondary cocktail beam was implanted into a 51 mm $\times$ 51 mm $\times$ 3 mm CeBr$_3$ detector positioned at the center of the experimental setup, approximately one meter downstream of three silicon PIN detectors of thicknesses 996 μm, 1041 μm, and 503 μm. The position and time of implanted ions as well as subsequent β-decay electrons and even low-energy γ rays were recorded by the CeBr$_3$ detector, which was optically coupled to a 52 mm $\times$ 52 mm Hamamatsu H13700 series Position Sensitive Photo-Multiplier Tube (PSPMT) [19]. The PSPMT was pixelated over a 16 $\times$ 16 grid, with all pixels read out as individual anode signals as well as a single dynode signal representing the summed energy output of all anode readouts. Decays were correlated to implanted ions using spatial and temporal information recorded by the PSPMT.

Fragments in the secondary beam were identified on an event-by-event basis using energy loss (ΔE) information in one of the silicon PIN detectors and the time of flight between the silicon PIN detector and a position-sensitive scintillator at the dispersive image of the A1900 fragment separator.

β-delayed γ rays were detected using two ancillary arrays surrounding the CeBr$_3$ implantation detector. The first array comprised 15 LaBr$_3$(Ce) detectors [20], each placed around the CeBr$_3$ in a ring perpendicular to the beam direction. The second array—the Segmented Germanium Array (SeGA) [21]—consisted of 16 HPGe detectors arranged in two concentric rings of eight detectors upstream and downstream of the CeBr$_3$ in the beta-SeGA configuration [22]. All events were read out using the NSCL Digital Data Acquisition System (DDAS) [23].

III. ANALYSIS

A. ^{37}Al β^- decay

The β-delayed γ-ray spectrum in Fig. 2 was produced using a β-decay ^{37}Al ion correlation window of 33.9 ms,

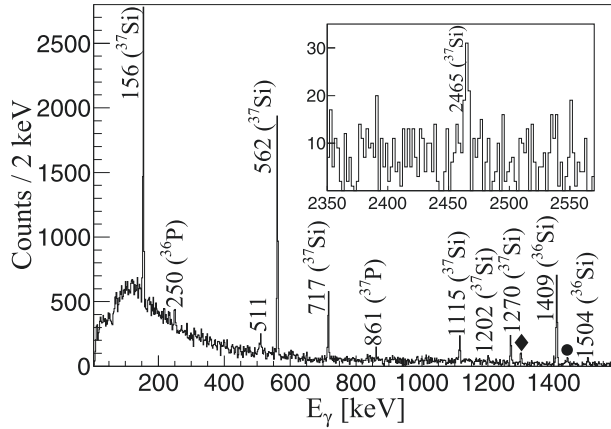FIG. 2. β-delayed γ-ray spectrum for γ rays detected in the SeGA detectors within a correlation window of 33.9 ms, which corresponds to three ^{37}Al β-decay half-lives ($T_{1/2} = 11.3$ ms). Previously observed γ-ray transitions in the ^{37}Si daughter [12,14,15] are labeled with their respective energies, as well as transitions in the β-delayed one-neutron emission ^{36}Si daughter and ^{36,37}P granddaughters. Other identified γ-ray transitions include the 1300 keV in ^{37}P (black diamond), the 1442 keV in ^{36}Si (black circle) and the 511 keV due to e^-e^+ annihilation. Inset: Region around newly observed 2465-keV γ-ray transition.

which corresponds to three ^{37}Al β-decay half-lives ($T_{1/2} = 11.3$ ms). The contribution of random correlations to the γ-ray spectrum was identified and subtracted to isolate β-delayed γ rays arising from ^{37}Al decay, using methods described in Refs. [14,24].

The transitions attributed to ^{37}Si in this work are in agreement with measurements from previous β-decay experiments in Refs. [14,15]. These include $\gamma - \gamma$ coincidences between the 562- and 1115-keV transitions and the 156-keV transition, confirming the presence of the 717- and 1270-keV positive-parity states preferentially populated in the β decay

TABLE I. Relative intensities of γ rays attributed to ^{36,37}Si observed in the SeGA detectors following the β decay of implanted ^{37}Al ions. The intensities are normalized to the intensity of the 156-keV transition in ^{37}Si and have been corrected for the SeGA detection efficiency simulated in GEANT4 [25]. γ-ray transitions in the ^{36}Si β^-n daughter have been identified with an asterisk. The intensities are compared with results presented in Ref. [14].

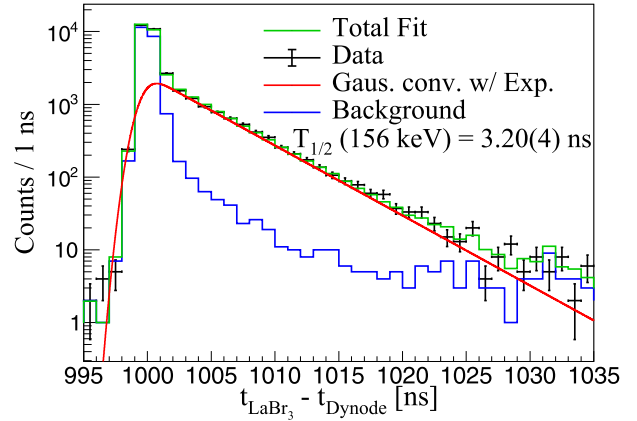| E_γ (keV)	$I_{\gamma,\text{exp.}}$	$I_{\gamma,\text{lit.}}$ [14]
155.8(2)	100(6)	100(4)
562.8(2)	88(5)	95(6)
716.6(2)	31(2)	40(4)
1115.0(3)	15(1)	14(4)
1201.5(3)	7(1)	11(4)
1269.6(2)	16(2)	16(4)
1409.2(2)*	59(4)	71(7)
1441.5(4)*	4(1)	9(3)
1503.8(3)*	4(1)	10(3)
2464.9(4)	2(1)	-

FIG. 3. Time difference distribution due to the half-life of the $(3/2_1^-)$ isomeric state in ^{37}Si (black). The best fit corresponding to a half-life of 3.20(4) ns shown in green is a linear combination of multiple convolutions (red) and a background region taken above the 156-keV transition (blue), scaled to the number of counts in the LaBr$_3$(Ce) energy region associated with the 156-keV γ-ray transition.

of ^{37}Al. These positive-parity states deexcite by γ rays that feed the negative-parity, low-lying states of interest. None of the other transitions observed in the one-neutron knockout reaction in Ref. [12] were identified in the γ-ray spectrum of this work. However, a 2465-keV γ ray was observed as shown in the inset of Fig. 2. A weak 1202-keV γ ray that deexcites the 1270-keV state in ^{37}Si is also observed in the γ-ray spectrum and is expected to populate the 68-keV state as discussed in Refs. [14,15]. The efficiency-corrected intensities of the γ rays attributed to ^{36}Si and ^{37}Si are presented in Table I, and normalized relative to the intensity of the 156-keV transition.

The 68-keV γ-ray transition that deexcites the $(7/2_1^-)$ state in ^{37}Si is unobserved following the β^- decay of ^{37}Al in this experiment. This is primarily due to the 68-keV state being weakly fed in the β^- decay of ^{37}Al [14]. Moreover, the high sensitivity of the CeBr$_3$ implantation detector to low-energy γ rays will most probably impede the detection of such a weak transition in surrounding γ-ray detectors.

Half-life measurement of the 156-keV state and technique validation

The half-life of the 156-keV state was previously extracted by broadened line shape analysis of the Doppler-reconstructed γ-ray spectrum in coincidence with ^{37}Si residues following a ^{9}Be(^{38}Si, ^{37}Si γ) reaction [12]. The utilization of the fast CeBr$_3$ and ancillary LaBr$_3$(Ce) detectors in this experimental setup allowed for the direct measurement of half-lives of isomeric states populated following the β decay of implanted ions, including the 156-keV state in ^{37}Si. The $\beta - \gamma$ fast-timing method [26] was employed to carry out this measurement by calculating the time difference for events where a β-decay electron correlated to a ^{37}Al ion was detected in the CeBr$_3$ implantation detector and a 156-keV γ ray was detected in one of the surrounding LaBr$_3$(Ce) detectors.

Figure 3 shows the time difference distribution associated with the population and subsequent depopulation of the isomeric 156-keV state in ^{37}Si. The time difference axis has been arbitrarily offset by 1000 ns, with the distribution taking the shape of a convolution of the prompt detector response, modeled using a Gaussian function, and the exponential decay of the 156-keV isomeric state of interest. A single fit does not properly account for the variation in the prompt time response as a function of the CeBr$_3$ dynode energy and is unable to accurately capture the time difference distribution to the left of the prompt Gaussian peak, systematically skewing the measured half-life to a shorter value. Accurately modeling the time difference distribution therefore calls for the linear combination of multiple convolutions, each varying as a function of the Gaussian width over the CeBr$_3$ dynode energy continuum [27].

The observed time difference distribution due to the half-life of the $(3/2_1^-)$ isomeric state was modeled using the linear combination of convolutions described in the previous paragraph, and a background region taken above the 156-keV peak region. The linear combination was then scaled to the number of counts in the LaBr$_3$(Ce) energy region associated with the 156-keV γ-ray transition.

Eleven time response functions combining the experimentally derived dynode energy Gaussian widths and exponential decay curves defined by different fixed half-lives were generated using the method described above and compared with experimental data to obtain χ^2 values [28]. The half-life corresponding to the minimum of a second-order polynomial function used to fit the distribution of the 11 χ^2 values was then used to generate the best time response function shown in green in Fig. 3. The half-life of the $(3/2_1^-)$ state in ^{37}Si and its associated statistical uncertainty at 1σ was determined to be 3.20(4) ns, which is in agreement with the previously measured half-life of 3.0(7) ns [12] with a factor of approximately 18 reduced statistical uncertainty. The reproduction of the half-life of the 156-keV state was used to validate the measurement technique for this dataset.

B. ^{38}Al β^-n decay

The feeding intensity of the 68-keV state in ^{37}Si is higher in the β^-n decay of ^{38}Al [14], such that γ rays corresponding to the ground-state transition can be observed in the β-delayed γ-ray spectrum correlated to ^{38}Al as shown in Fig. 4. The 1470-1159-1074 keV γ-ray cascade previously observed in the ^{38}Al β-decay experiment in Ref. [14] is also confirmed in this work. Table II shows the relative intensities of the γ rays observed in the SeGA detectors and attributed to the ^{38}Si daughter and the ^{37}Si β^-n daughter. The intensities were efficiency corrected and normalized to that of the 1074-keV γ ray in ^{38}Si.

As highlighted in Fig. 4, a 68-keV photopeak is clearly observed in the γ-ray spectrum correlated to the ^{38}Al ions. Arguments have been made in Sec. III A and Refs. [14,15] concerning the placement of a corresponding 68-keV state in ^{37}Si as well as the nonobservation of a 68-keV photopeak in the β-delayed γ-ray spectrum correlated to ^{37}Al. The nonobservation of transitions assigned to the ^{38}Si daughter in
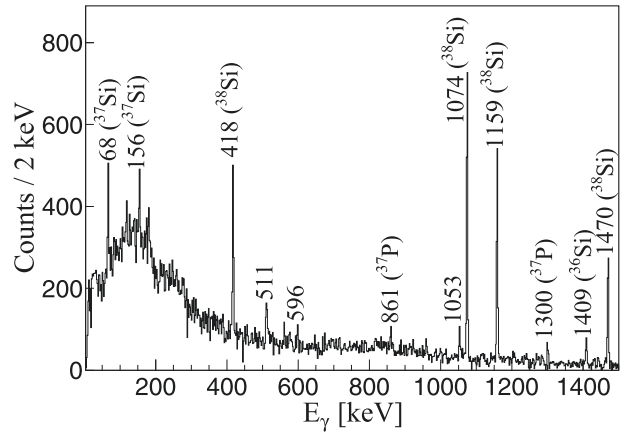

FIG. 4. β-delayed γ-ray spectrum for γ rays detected in the SeGA detectors within a correlation window of 27 ms, which corresponds to three ^{38}Al β-decay half-lives (T$_{1/2}$ = 9 ms). Previously observed γ-ray transitions in the ^{38}Si daughter and the ^{37}Si β-delayed one-neutron emission daughter are labeled with their respective energies. Transitions attributed to ^{36}Si and ^{37}P are also identified as well as the 511 keV due to e^-e^+ annihilation and 596 keV due to (n, n', γ) reactions on ^{74}Ge nuclei of the HPGe detectors. A currently unplaced 1053-keV γ-ray transition is also observed.

$\gamma - \gamma$ coincidence measurements with the 68-keV transition following the β^-n decay of ^{38}Al in this work supports the attribution of this γ ray to the 68-keV state in ^{37}Si as its most probable origin.

Half-life measurement of the 68-keV state

Prior to this work, the half-life of the 68-keV state was unknown. The validated technique discussed in Sec. III A was similarly employed to measure its half-life, given the presence of implanted ^{38}Al ions during this experiment. The half-life of the $(7/2_1^-)$ isomeric state in ^{37}Si and its associated statistical

TABLE II. Relative intensities of γ rays attributed to ^{37,38}Si observed in the SeGA detectors following the β decay of implanted ^{38}Al ions. The intensities are normalized to the intensity of the 1074-keV transition in ^{38}Si and have been corrected for the SeGA detection efficiency simulated in GEANT4. The γ-ray transitions in ^{37}Si are identified with an asterisk and all relative intensities are compared with results presented in Ref. [14]. The significant uncertainty in the relative intensity of the 68-keV γ ray is attributed to the large detection efficiency uncertainty for γ rays with energies below 100 keV in this experiment.

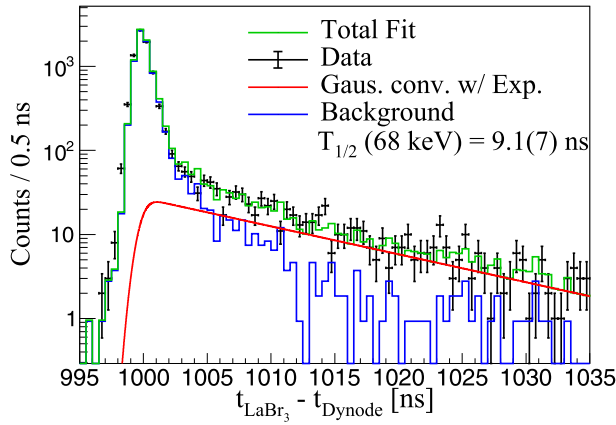| E_γ (keV)	$I_{\gamma,\mathrm{exp.}}$	$I_{\gamma,\mathrm{lit.}}$ [14]
67.9(2)*	500(200)	>7
155.5(3)*	12(3)	15(7)
417.9(2)	33(4)	32(5)
1074.3(2)	100(7)	100(12)
1158.7(2)	74(7)	59(7)
1470.0(2)	46(5)	42(5)

FIG. 5. Time difference distribution due to the half-life of the $(7/2^-)$ isomeric state in ^{37}Si (black). The best fit corresponding to a half-life of 9.1(7) ns shown in green is a linear combination of multiple convolutions (red) and a background region above the 68 keV transition (blue), scaled to the number of counts in the LaBr$_3$(Ce) energy region associated with the 68-keV γ-ray transition.

uncertainty at 1σ was measured as 9.1(7) ns as shown in Fig. 5.

IV. DISCUSSION

The experimental level scheme of ^{37}Si is shown in Fig. 6 compared to predictions from shell model calculations using the SDPF-MU [16], SDPF-U-SI [17], and FSU [29] Hamiltonians up to the one-neutron separation energy of 2.21(13) MeV [30]. Tentative experimental spin-parity assignments were obtained from Refs. [14,15]. Theoretical negative-parity states shown in Fig. 6 were calculated by restricting protons to the sd shell, and neutrons to the fp shell. Positive-parity states were calculated with the FSU Hamiltonian by allowing one nucleon to be excited from the sd to fp shell. These are shown in the far-right portion of Fig. 6.

The measured half-lives of the $(7/2_1^-)$ and $(3/2_1^-)$ states are shown in Table III, as well as their reduced ground-state transition probabilities. A comparison to shell model calculations indicates that the experimental $B(M1)$ values for both $(7/2_1^-)$ $\rightarrow (5/2_{g.s.}^-)$ and $(3/2_1^-) \rightarrow (5/2_{g.s.}^-)$ transitions lie between the SDPF-MU and SDPF-U-SI predictions. A pure $M1$ decay was assumed for both transitions given theoretical expectations of small $E2/M1$ mixing, and as such, the experimental $B(M1)$ values are considered as upper limits. The experiment versus theory comparisons in this work can be further investigated in light of a survey of similar comparisons for low-lying excited
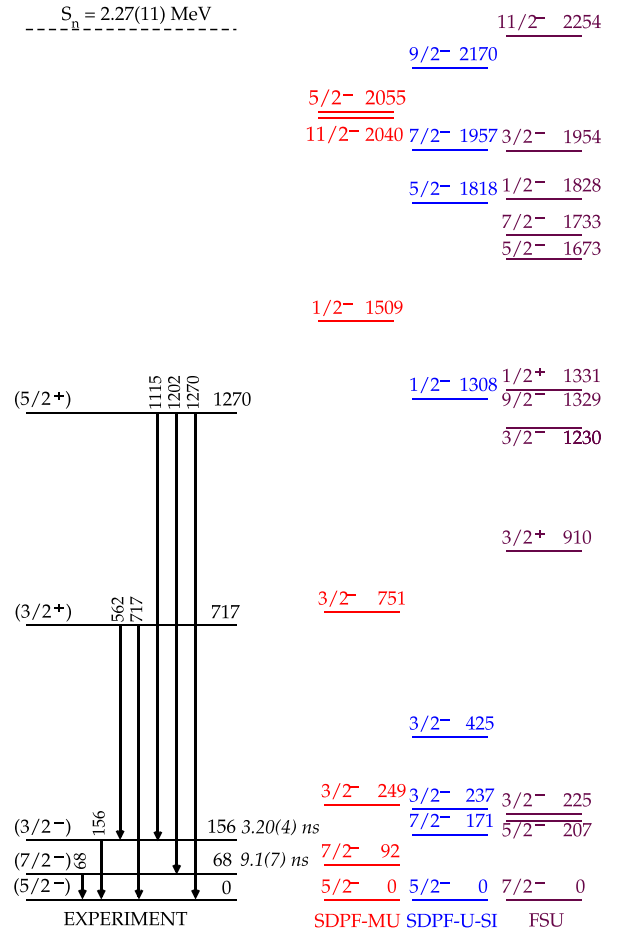

FIG. 6. Comparison of the ^{37}Si experimental level scheme (black) to theoretical level schemes predicted by shell model calculations using the SDPF-MU (red), SDPF-U-SI (blue), and FSU (maroon) interactions up to the one-neutron separation energy of ^{37}Si. Experimental spin-parity assignments in parentheses are tentative and taken from Refs. [14,15], and the newly measured half-lives of the low-lying excited states are included to the right of their corresponding levels in italics.

to ground-state $M1$ transition matrix elements evaluated for sd-shell nuclei between $A = 16$ and $A = 40$, as discussed in Ref. [31].

Consequently, the measured $B(M1)$ values were converted into reduced $M1$ transition matrix elements, $M(M1)$ using the

TABLE III. Half-lives and reduced ground-state transition probabilities from the $(7/2_1^-)$ and $(3/2_1^-)$ states in ^{37}Si.

			$B(M1)$		
Transition	Energy (keV)	Exp. T$_{1/2}$ (ns)	Exp. (μ_N^2)	SDPF-MU (μ_N^2)	SDPF-U-SI (μ_N^2)
$(7/2_1^-) \rightarrow (5/2_{g.s.}^-)$	67.9(2)	9.1(7)	0.0137(11)	0.0369	0.0007
$(3/2_1^-) \rightarrow (5/2_{g.s.}^-)$	155.8(2)	3.20(4)	0.00325(10)	0.0178	0.0005

TABLE IV. Comparisons between experimental and theoretical matrix elements for low-lying ground-state $M1$ transitions in ^{37}Si.

Transition	Energy (keV)	$M(M1)$		
		Exp. (μ_N)	SDPF-MU (μ_N)	SDPF-U-SI (μ_N)
$(7/2_1^-) \rightarrow (5/2_{g.s.}^-)$	67.9(2)	0.33(3)	0.54	0.076
$(3/2_1^-) \rightarrow (5/2_{g.s.}^-)$	155.8(2)	0.114(1)	0.268	0.044

relationship:

$$M(M1) = |\sqrt{B(M1) \times (2J_i + 1)}|, \quad (1)$$

where J_i represents the spin assigned to the initial state undergoing deexcitation. The experimental $M(M1)$ values are presented in Table IV and compare reasonably well to shell model calculations, consistent with findings for other sd-shell nuclei as presented in Ref. [31] for such degree of smallness of measured $B(M1)$ values.

The structure of the $(7/2_1^-)$ and $(3/2_1^-)$ isomeric states in ^{37}Si can be compared to each other. Table V contains the fp-shell neutron occupation numbers calculated for both isomeric states and the ground state in ^{37}Si using the SDPF-MU and SDPF-U-SI interactions. Both calculations predict the $(5/2_{g.s.}^-)$ and $(7/2_1^-)$ states to be dominated by the $(\nu f_{7/2})^3$ configuration unlike the $(3/2_1^-)$ state which is predicted to have a mixing of the $(\nu f_{7/2})^3$ and $(\nu f_{7/2})^2 \otimes (\nu p_{3/2})^1$ configurations.

TABLE V. Neutron occupation numbers for the $5/2_{g.s.}^-$, $7/2_1^-$, and $3/2_1^-$ states in the fp shell.

Interaction	J^π	$0f_{7/2}$	$0f_{5/2}$	$1p_{3/2}$	$1p_{1/2}$
SDPF-MU	$5/2_{g.s}^-$	2.63	0.14	0.21	0.02
	$7/2_1^-$	2.68	0.12	0.18	0.02
	$3/2_1^-$	2.30	0.08	0.58	0.05
SDPF-U-SI	$5/2_{g.s}^-$	2.61	0.08	0.28	0.03
	$7/2_1^-$	2.73	0.10	0.14	0.02
	$3/2_1^-$	2.16	0.06	0.74	0.04

V. CONCLUSIONS

Low-lying $(7/2_1^-)$ and $(3/2_1^-)$ isomeric states at 68 and 156 keV in ^{37}Si were studied at NSCL following their population in the β^-n and β^- decay of implanted ^{38}Al and ^{37}Al ions, respectively. New structure information including the half-life of the 68-keV state was measured as 9.1(7) ns as well as the ground-state transition strength, $B(M1)$ measured as 0.0137(11) μ_N^2, assuming a pure $M1$ transition. Similar measurements for the 156-keV transition were also carried out, with the half-life and $B(M1)$ strength measured as 3.20(4) ns and 0.00325(10) μ_N^2, respectively, and found to be in agreement with a previous measurement. The experimental results were found to be consistent with large-scale shell model predictions. The characterization of these isomeric states in ^{37}Si validates shell model predictions of closely lying excited isomeric states in neutron-rich odd-A Si isotopes approaching the $N = 28$ shell gap.

[1] T. Otsuka, R. Fujimoto, Y. Utsuno, B. A. Brown, M. Honma, and T. Mizusaki, Phys. Rev. Lett. **87**, 082502 (2001).

[2] T. Otsuka, Phys. Scr. **2013**, 014007 (2013).

[3] T. Glasmacher, B. Brown, M. Chromik, P. Cottle, M. Fauerbach, R. Ibbotson, K. Kemper, D. Morrissey, H. Scheit, D. Sklenicka, and M. Steiner, Phys. Lett. B **395**, 163 (1997).

[4] O. Sorlin and M.-G. Porquet, Prog. Part. Nucl. Phys. **61**, 602 (2008).

[5] N. Iwasa, T. Motobayashi, H. Sakurai, H. Akiyoshi, Y. Ando, N. Aoi, H. Baba, N. Fukuda, Z. Fülöp, U. Futakami, T. Gomi, Y. Higurashi, K. Ieki, H. Iwasaki, T. Kubo, S. Kubono, H. Kinugawa, H. Kumagai, M. Kunibu, S. Michimasa *et al.*, Phys. Rev. C **67**, 064315 (2003).

[6] S. Takeuchi, M. Matsushita, N. Aoi, P. Doornenbal, K. Li, T. Motobayashi, H. Scheit, D. Steppenbeck, H. Wang, H. Baba, D. Bazin, L. Càceres, H. Crawford, P. Fallon, R. Gernhäuser, J. Gibelin, S. Go, S. Grévy, C. Hinke, C. R. Hoffman *et al.*, Phys. Rev. Lett. **109**, 182501 (2012).

[7] R. W. Ibbotson, T. Glasmacher, B. A. Brown, L. Chen, M. J. Chromik, P. D. Cottle, M. Fauerbach, K. W. Kemper, D. J. Morrissey, H. Scheit, and M. Thoennessen, Phys. Rev. Lett. **80**, 2081 (1998).

[8] C. Force, S. Grévy, L. Gaudefroy, O. Sorlin, L. Caceres, F. Rotaru, J. Mrazek, N. L. Achouri, J. C. Angèlique, F. Azaiez, B. Bastin, R. Borcea, A. Buta, J. M. Daugas, Z. Dlouhy, Z. Dombràdi, F. DeOliveira, F. Negoita, Y. Penionzhkevich,

M. G. Saint-Laurent *et al.*, Phys. Rev. Lett. **105**, 102501 (2010).

[9] S. Paschalis, P. Fallon, A. O. Macchiavelli, M. Petri, P. C. Bender, M. P. Carpenter, X. Chen, C. J. Chiara, R. M. Clark, M. Cromaz, S. Gros, L. Hamilton, C. R. Hoffman, R. V. F. Janssens, T. Lauritsen, I. Y. Lee, C. J. Lister, E. A. McCutchan, L. Phair, W. Reviol *et al.*, J. Phys.: Conf. Ser. **312**, 092050 (2011).

[10] F. Rotaru, F. Negoita, S. Grévy, J. Mrazek, S. Lukyanov, F. Nowacki, A. Poves, O. Sorlin, C. Borcea, R. Borcea, A. Buta, L. Cáceres, S. Calinescu, R. Chevrier, Z. Dombrádi, J. M. Daugas, D. Lebhertz, Y. Penionzhkevich, C. Petrone, D. Sohler *et al.*, Phys. Rev. Lett. **109**, 092503 (2012).

[11] S. Nummela, P. Baumann, E. Caurier, P. Dessagne, A. Jokinen, A. Knipper, G. Le Scornet, C. Miehé, F. Nowacki, M. Oinonen, Z. Radivojevic, M. Ramdhane, G. Walter, and J. Äystö, Phys. Rev. C **63**, 044316 (2001).

[12] S. R. Stroberg, A. Gade, J. A. Tostevin, V. M. Bader, T. Baugher, D. Bazin, J. S. Berryman, B. A. Brown, C. M. Campbell, K. W. Kemper, C. Langer, E. Lunderberg, A. Lemasson, S. Noji, F. Recchia, C. Walz, D. Weisshaar, and S. J. Williams, Phys. Rev. C **90**, 034301 (2014).

[13] S. R. Stroberg, A. Gade, J. A. Tostevin, V. M. Bader, T. Baugher, D. Bazin, J. S. Berryman, B. A. Brown, C. M. Campbell, K. W. Kemper, C. Langer, E. Lunderberg, A. Lemasson, S. Noji, T. Otsuka, F. Recchia, C. Walz, D. Weisshaar, and S. Williams, Phys. Rev. C **91**, 041302(R) (2015).

[14] K. Steiger, S. Nishimura, Z. Li, R. Gernhäuser, Y. Utsuno, R. Chen, T. Faestermann, C. Hinke, R. Krücken, M. Kurata-Nishimura, G. Lorusso, Y. Miyashita, N. Shimizu, K. Sugimoto, T. Sumikama, H. Watanabe, and K. Yoshinaga, Eur. Phys. J. A **51**, 117 (2015).

[15] B. Abromeit, V. Tripathi, H. L. Crawford, S. N. Liddick, S. Yoshida, Y. Utsuno, P. C. Bender, B. P. Crider, R. Dungan, P. Fallon, K. Kravvaris, N. Larson, R. S. Lubna, T. Otsuka, C. J. Prokop, A. L. Richard, N. Shimizu, S. L. Tabor, and A. Volya, Phys. Rev. C **100**, 014323 (2019).

[16] Y. Utsuno, T. Otsuka, B. A. Brown, M. Honma, T. Mizusaki, and N. Shimizu, Phys. Rev. C **86**, 051301(R) (2012).

[17] F. Nowacki and A. Poves, Phys. Rev. C **79**, 014310 (2009).

[18] D. Morrissey, B. Sherrill, M. Steiner, A. Stolz, and I. Wiedenhoever, Nucl. Instrum. Meth. Phys. Res. B **204**, 90 (2003).

[19] Data Sheet, *Flat Panel Type Mutlianode PMT Assembly H13700 Series*, Hamamatsu Photonics KK, 314-5, Shimokanzo, Iwata City, Shizuoka Pref., 438-0193, Japan, 2020, retrieved from: https://www.hamamatsu.com/resources/pdf/etd/H13700_TPMH1370E.pdf, accessed 2 April 2021.

[20] B. Longfellow, P. Bender, J. Belarge, A. Gade, and D. Weisshaar, Nucl. Instrum. Meth. Phys. Res. A **916**, 141 (2019).

[21] W. Mueller, J. Church, T. Glasmacher, D. Gutknecht, G. Hackman, P. Hansen, Z. Hu, K. Miller, and P. Quirin, Nucl. Instrum. Meth. Phys. Res. A **466**, 492 (2001).

[22] O. Shehu, B. Crider, T. Ginter, C. Hoffman, T. Ogunbeku, Y. Xiao, K. Childers, P. Chowdhury, C. Fry, E. Lamere, R. Lewis, S. Liddick, B. Longfellow, S. Lyons, S. Neupane, D. Pérez-Loureiro, C. Prokop, A. Richard, U. Silwal, D. Siwakoti *et al.*, Nucl. Instrum. Meth. Phys. Res. A **1035**, 166789 (2022).

[23] C. Prokop, S. Liddick, B. Abromeit, A. Chemey, N. Larson, S. Suchyta, and J. Tompkins, Nucl. Instrum. Meth. Phys. Res. A **741**, 163 (2014).

[24] T. Kurtukian-Nieto, J. Benlliure, and K.-H. Schmidt, Nucl. Instrum. Meth. Phys. Res. A **589**, 472 (2008).

[25] S. Agostinelli, J. Allison, K. Amako, J. Apostolakis, H. Araujo, P. Arce, M. Asai, D. Axen, S. Banerjee, G. Barrand, F. Behner, L. Bellagamba, J. Boudreau, L. Broglia, A. Brunengo, H. Burkhardt, S. Chauvie, J. Chuma, R. Chytracek, G. Cooperman *et al.*, Nucl. Instrum. Meth. Phys. Res. A **506**, 250 (2003).

[26] H. Mach, R. Gill, and M. Moszyński, Nucl. Instrum. Meth. Phys. Res. A **280**, 49 (1989).

[27] B. Crider, C. Prokop, S. Liddick, H. Albers, M. Alshudifat, A. Ayangeakaa, M. Carpenter, J. Carroll, J. Chen, C. Chiara, A. Dombos, S. Go, R. Grzywacz, J. Harker, R. Janssens, N. Larson, T. Lauritsen, R. Lewis, S. Quinn, F. Recchia *et al.*, Nucl. Instrum. Meth. Phys. Res. A **1055**, 168525 (2023).

[28] P. R. Bevington and D. K. Robinson, *Data Reduction and Error Analysis for the Physical Sciences*, 3rd ed. (McGraw-Hill, Boston, 2003)

[29] R. S. Lubna, K. Kravvaris, S. L. Tabor, V. Tripathi, E. Rubino, and A. Volya, Phys. Rev. Res. **2**, 043342 (2020).

[30] M. Wang, W. Huang, F. Kondev, G. Audi, and S. Naimi, Chin. Phys. C **45**, 030003 (2021).

[31] W. A. Richter, S. Mkhize, and B. A. Brown, Phys. Rev. C **78**, 064302 (2008).